

Spectral polarization-encoding of broadband laser pulses by optical rotatory dispersion and its applications in spectral manipulation

Xiaowei Lu(陆小微), Congying Wang(王聪颖), Xuanke Zeng(曾选科), Jiahe Lin(林家和), Yi Cai(蔡懿), Qinggang Lin(林庆钢), Shangguan Shangguan(上官煌城), Zhenkuan Chen(陈振宽), Shixiang Xu(徐世祥), and Jingzhen Li(李景镇)

Citation: Chin. Phys. B, 2021, 30 (**7**): 077801. DOI: 10.1088/1674-1056/abf0fb
Journal homepage: http://cpb.iphy.ac.cn; http://iopscience.iop.org/cpb

What follows is a list of articles you may be interested in

Temperature dependent terahertz giant anisotropy and cycloidal spin wave modes in $BiFeO_3$ single crystal

Fan Liu(刘凡), Zuanming Jin(金钻明), Xiumei Liu(刘秀梅), Yuqing Fang(方雨青), Jiajia Guo(国家嘉), Yan Peng(彭滟), Zhenxiang Cheng(程振祥), Guohong Ma(马国宏), Yiming Zhu(朱亦鸣)
Chin. Phys. B, 2020, 29 (**7**): 077804. DOI: 10.1088/1674-1056/ab8dae

Single-shot measurement of THz pulses

Lei Yang(杨磊), Lei Hou(侯磊), Chengang Dong(董陈岗), Wei Shi(施卫)
Chin. Phys. B, 2020, 29 (**5**): 057803. DOI: 10.1088/1674-1056/ab821f

Review of ultrafast spectroscopy studies of valley carrier dynamics in two-dimensional semiconducting transition metal dichalcogenides

Dong Sun(孙栋), Jia-Wei Lai(赖佳伟), Jun-Chao Ma(马骏超), Qin-Sheng Wang(王钦生), Jing Liu (刘晶)
Chin. Phys. B, 2017, 26 (**3**): 037801. DOI: 10.1088/1674-1056/26/3/037801

Photo-induced intramolecular electron transfer and intramolecular vibrational relaxation of rhodamine 6G in DMSO revealed by multiplex transient grating spectroscopy

Jiang Li-Lin, Liu Wei-Long, Song Yun-Fei, Sun Shan-Lin
Chin. Phys. B, 2014, 23 (**10**): 107802. DOI: 10.1088/1674-1056/23/10/107802

Selective excitation of molecular mode in a mixture by femtosecond resonance-enhanced coherent anti-Stokes Raman scattering spectroscopy

He Ping,Li Si-Ning,Fan Rong-Wei,Li Xiao-Hui,Xia Yuan-Qin,Yu Xin,Chen De-Ying
Chin. Phys. B, 2012, 21 (**2**): 027801. DOI: 10.1088/1674-1056/21/2/027801

Spectral polarization-encoding of broadband laser pulses by optical rotatory dispersion and its applications in spectral manipulation*

Xiaowei Lu(陆小微)[1], Congying Wang(王聪颖)[1], Xuanke Zeng(曾选科)[1], Jiahe Lin(林家和)[1], Yi Cai(蔡懿)[1,†], Qinggang Lin(林庆钢)[1], Huangcheng Shangguan(上官煌城)[1], Zhenkuan Chen(陈振宽)[1,2], Shixiang Xu(徐世祥)[1], and Jingzhen Li(李景镇)[1]

[1] *Shenzhen Key Laboratory of Micro-Nano Photonic Information Technology, Key Laboratory of Optoelectronic Devices and Systems of Ministry of Education and Guangdong Province, College of Physics and Optoelectronics Engineering, Shenzhen University, Shenzhen* 518060, *China*

[2] *Collaborative Innovation Center for Optoelectronic Science and Technology, International Collaborative Laboratory of 2D Materials for Optoelectronics Science and Technology (Ministry of Education), Institute of Microscale Optoelectronics, Shenzhen University, Shenzhen* 518060, *China*

(Received 8 February 2021; revised manuscript received 4 March 2021; accepted manuscript online 23 March 2021)

We propose a kind of spectral polarization-encoding (SPE) for broadband light pulses, which is realized by inducing optical rotatory dispersion (ORD), and decoded by compensating ORD. Combining with polarization-sensitive devices, SPE can not only work to control polarization-dependent transmission for central wavelength or bandwidth-tunable filtering, but also can be used for broadband regenerative or multi-pass amplification with a polarization-dependent gain medium to improve output bandwidth. SPE is entirely passive thus very simple to be designed and aligned. By using an ORD crystal with a good transmission beyond 3-μm mid-infrared region, *e.g.*, $AgGaS_2$, SPE promises to be applied for the wavelength tuning lasers in mid-infrared region, where the tunning devices are rather under developed compared with those in visible and near-infrared region.

Keywords: ultrafast optics, optical rotatory dispersion, spectral polarization-encoding, spectral manipulation

PACS: 78.47.J–, 42.25.Ja, 42.79.–e, 42.60.–v **DOI:** 10.1088/1674-1056/abf0fb

1. Introduction

It is well known that ultrashort light pulses have inherent broad spectral bandwidth, which provides us with great convenience to implement spectral manipulation or shaping. Consequently, femtosecond pulse shaping has attracted an increased interest due to its important applications in many fields including ultrahigh speed communications,[1,2] ultrafast optical signal processing and computing,[3] ultrafast nonlinear processes,[4,5] ultrafast optical imaging,[6,7] precise optical metrology,[8,9] quantum coherent control,[10] high efficient terahertz pulse generation,[11] and chirped-pulse amplification (CPA).[12,13] Until now, many methods for femtosecond pulse shaping have been reported. For example, spatial light modulator[14] and fiber Bragg grating[15] were used for ultrahigh speed communications, whereas etalons,[16] wavelength-dependent reflectors,[17] birefringent plates,[18] and acousto-optical programmable dispersive filters[19] were applied in CPA systems to alleviate spectral narrowing effects.

This paper proposes a novel way to implement femtosecond pulse shaping, which, similar to the spectral time-encoding in CPA, is a kind of spectral polarization-encoding (SPE) for ultrashort light pulses. SPE can be realized simply by allowing a linearly polarized broadband light pulse through some optically active crystals to induce some optically rotatory dispersions (ORD). As a result, all spectral components of the ultrashort pulse are still linearly polarized but their polarization directions can be manipulated by controlling the ORD. This SPE can be decoded by compensating ORD, which is important for some of its applications, *e.g.*, broadband light pulse amplification, spectral shaping, and so on.

2. Theory and proof-in-principle experiments

An ultrashort light pulse has inherently very affluent spectral components. For a transform-limited pulse, when it propagates through a disperser, it becomes a chirped pulse, and its affluent spectrum allows its temporal duration to be stretched. As a result, in different temporal slices, one will "see" different frequencies inside the chirped pulse. This process can be regarded as a spectral time-encoding. Traditionally, these spectral components have an identical polarization. However, polarization is one of the most important freedoms of a light pulse, so it is very interesting to encode the polarization direction of all the spectral components of an ultrashort light pulse, which, fortunately, can be simply realized by inducing ORD.

As we know, a linearly polarized light beam can be seen as the overlap of left circularly polarized and right circularly

*Project supported by the National Natural Science Foundation of China (Grant Nos. 92050203, 62075138, 61827815, and 61775142) and Shenzhen Fundamental Research Project (Grant Nos. JCYJ20190808164007485, JCYJ20190808121817100, JSGG20191231144201722, and JCYJ20190808115601653).

†Corresponding author. E-mail: caiyi@szu.edu.cn

© 2021 Chinese Physical Society and IOP Publishing Ltd

polarized components. When the beam goes through an ORD medium, the two components will travel with different velocities. Consequently, the output beam still keeps its linear polarization but rotates its polarization direction by a wavelength-dependent angle with regard to that of the input beam due to ORD. Consequently, we can actualize SPE for a broadband pulse. One of the simple ways to induce ORD is to allow a light pulse through some optically active substances. It is an entirely passive method and very easy to be aligned, meanwhile, unlike the magnetic ORD due to Faraday effect, it works without need of any applied fields.

When a linearly polarized beam at wavelength of λ passes through an optically active substance with thickness of L, the rotating angle can be expressed as

$$\alpha(\lambda) = \eta(\lambda)L. \tag{1}$$

Here $\alpha(\lambda)$ and $\eta(\lambda)$ stand for rotating angle and rotation coefficient, respectively. Both of them are wavelength-dependent. One can see that ORD stems from $\eta(\lambda)$ is proportional to the thickness L. Accordingly, if the input is a linearly polarized pulse with broad bandwidth, after through an ORD crystal, different spectral components of the pulse correspond to different polarizations, *i.e.*, SPE. Obviously, we can manipulate SPE or $\alpha(\lambda)$ by changing $\eta(\lambda)$ or/and L of an optically active crystal.

The ORD generated by this way is compensable, so our SPE can be decoded, which is important in some applications, *e.g.* broadband pulse amplification. One way to compensate ORD is to allow the broadband pulses with ORD through another optically active substance which has a rotation coefficient of $-\eta(\lambda)$ and an equal thickness of the crystal to generate ORD (Fig. 1(a)). Fortunately, this compensation is practicable because some of the optically active substances, *e.g.*, quartz, have two mirror-symmetrical configurations: the left-handed and the right-handed, which have opposite values of $\eta(\lambda)$ with each other. We call this decoding method as LR method. Another way to realize ORD compensation is shown in Fig. 1(b) including only single crystal puls a mirror, which we call SCM method. There, the ORD is generated from the first pass through a piece of rotatory crystal, and can be compensated automatically to bounce the beam back through the same crystal again with a mirror.

Besides these two ways, we propose another way to compensate ORD, which, as shown in Fig. 1(c), includes double complete same ORD plates plus a broadband half-wave plate (BHW) between the two plates, and we call this decoding as DCW method. It is an all-transmission method which combines the advantages of the two other methods. Here the BHW is firstly aligned so that its fast or slow axis along with the polarization direction of input pulse without the ORD crystal (ORDC) there. Suppose the ORDC will rotate the polarization direction of its incident light pulse with an angle of $\alpha(\lambda)$, the light beam will pass though the BHW following the ORDC with a cross angle of $\alpha(\lambda)$ between its polarization direction and the fast or slow axis of the BHW. After passing through the BHW, the rotation angle becomes $-\alpha(\lambda)$ or π–$\alpha(\lambda)$, which means that the ORD can be removed by inducing another rotatory angle $\alpha(\lambda)$, or passing through another complete same ORD crystal as the first one. If the fast axis of BHW is at an arbitrary angle θ relative to the input polarization, after passing through BHW, the polarization direction is 2θ–$\alpha(\lambda)$, SPE can also be decoded by the second ORDC, except the polarization direction rotates to 2θ.

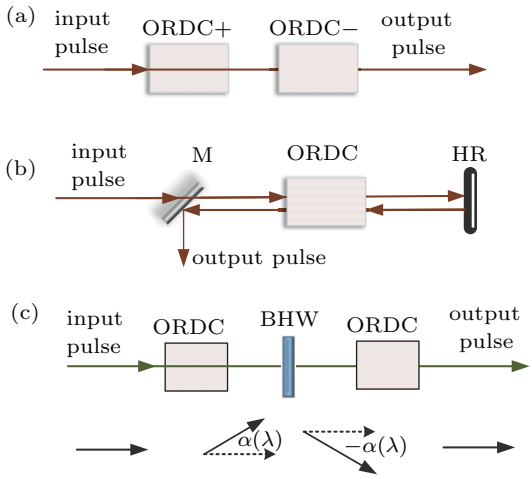


Fig. 1. The ways to compensate ORD: (a) using another crystal with mirror-symmetrical configuration (LR), (b) reflecting the light beam back to the substance (SCM), or (c) using two complete same ORD plates plus a broadband half-wave plate (DCW). ORDC: ORD crystal; ORDC+ and ORDC–: two ORD plates with the same ORD value but opposite signs; BHW: broadband half-wave plate; M: mirror; HR: 0° high reflective mirror.

Proof-in-principle experiments are implemented for three decoding methods as shown in Fig. 1, using a commercial femtosecond laser oscillator (Mirca-5, Coherent Co.) as the light resource. The oscillator exports 80 MHz, 780 nm, 400 mW pulse chain with a tunable bandwidth from 60 nm to 100 nm. A piece of left-handed quartz with a thickness of 20 mm is used for encoding. The rotation coefficient of quartz at 0.78 μm is about 12 deg/mm, and the rotating angle at 0.78 μm is $\alpha(0.78\ \mu\text{m}) = 241$ deg. After encoding, the wavelength-dependent rotating angle of the polarization is shown by the purple line in Fig. 2. When wavelength varies from 0.72 to 0.88 μm, the rotating angle decreases from 285.1 deg to 187.6 deg, close to a linear trend. Another 20-mm quartz with the opposite/same chirality is used for decoding in the configures of LR or DCW, respectively. All the elements, including the mirrors and the wave plate, are using broadband design. By applying a linear polarizer and a spectrograph (HR4000, Ocean Optics, Inc.) at the output side in the three designs respectively, the output spectra (solid lines) and the corresponding transmissions (dotted lines) are shown in Fig. 2. The thick gray line stands for the input spectrum. It is obvious that

the compensated spectra coincide well with the original one and their transmissions are nearly constant of 1 (normalized), which shows that all three designs can operate well for SPE decoding.

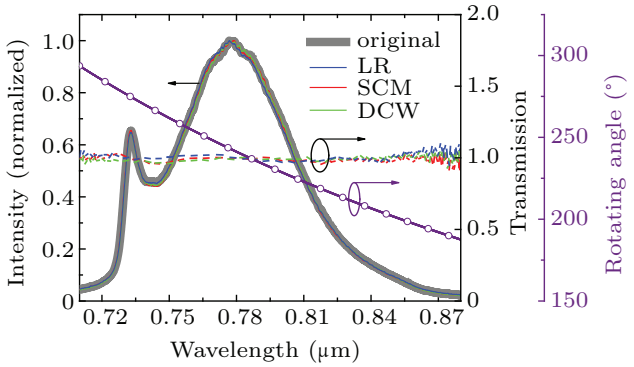


Fig. 2. Experimental ORD compensation results for LR (blue lines), SCM (red lines), and DCW (green lines), solid lines are spectra *versus* wavelength and dotted lines are transmission *versus* wavelength.

3. Applications

3.1. Spectra shaping

It is well known the transmission of a linear polarizer is polarization-dependent, so SPE by the aid of a polarizer can work to manipulate wavelength-dependent transmission, thereby realize the spectra shaping of broadband pulses.

As shown in Fig. 3, when a linearly polarized broadband pulse passes through a BHW and an ORDC, each spectral component of the pulse has its own polarization direction due to ORD, thereby has its own transmission. Here the BHW before the ORDC is used to rotate the polarization directions of all input spectral components with an identical angle $(-\alpha_0)$, thus the spectral component (λ_0) with the maximal transmission can be chosen flexibly. The rotatory angle after the ORDC and BHW is

$$\alpha'(\lambda) = \eta(\lambda)L - \alpha_0 = \alpha(\lambda) - \alpha_0. \tag{2}$$

Accordingly, the spectral/polarization-dependent transmission of the linear polarizer can be expressed as

$$T(\lambda) = \cos^2[\eta(\lambda)L - \alpha_0] \quad \text{or} \quad \cos^2[\alpha(\lambda) - \alpha_0]. \tag{3}$$

Figure 4(a) shows the transmission curves $T(\lambda)$ of the setup in Fig. 3 *versus* wavelength (μm) by using a quartz plate as ORD crystal (black: $L = 5.0$ mm; red: $L = 10.0$ mm; blue: $L = 15.0$ mm; green: $L = 20.0$ mm; purple: $L = 40$ mm) when setting α_0 at $\lambda = 0.75$ μm. We can see for a fixed α_0, the transmission bandwidth decreases with the thickness of the quartz crystal. Accordingly, if using a wedge pair instead of the quartz plate to make the thickness to be alterable, the setup in Fig. 3 can work as a bandwidth-tunable filter. Figure 4(b) shows the shift of the transmission peaks by simply rotating the BHW at different α_0 with a 40-mm-quartz as an encoding ORDC. It can be seen obviously that there are multiple transmission peaks in Fig. 4(b), and for normal use of the filter, the adjacent interval should be larger than the pulse width. Applying such a spectra shaper to our laser, wavelength-tunable output can easily be realized. Confirmatory experiments are carried out where an 80-MHz, 2.5-nJ pulse with a tunable bandwidth from 60 nm to 100 nm is used as the input and the results are shown in Fig. 4(c), where the experimental output spectra (dots) are consistent well with the calculative results (lines). Although the transmissions have multi-peak structure, however, the "free spectrum range", or the interval between adjacent peaks, is up to 156 nm, which is much wider than the spectral width (72.1 nm) of the laser we used here. Therefore, output spectra present single-peak structures, and the bandwidth is as broad as about 43 nm.

In addition, the ORD profile can be altered by combination of multiple ORD crystals. The black line in Fig. 5 presents the spectral-dependent rotatory angle of a quartz plate with a thickness of 4.5 mm. One can see that from visible to near-infrared (near-IR), as those of many optically active substances, the $|\alpha(\lambda)|$ of quartz decreases with wavelength.



Fig. 3. The setup for spectral shaping. BHW: broadband half-wave plate; ORDC: optically rotatory dispersion crystal.

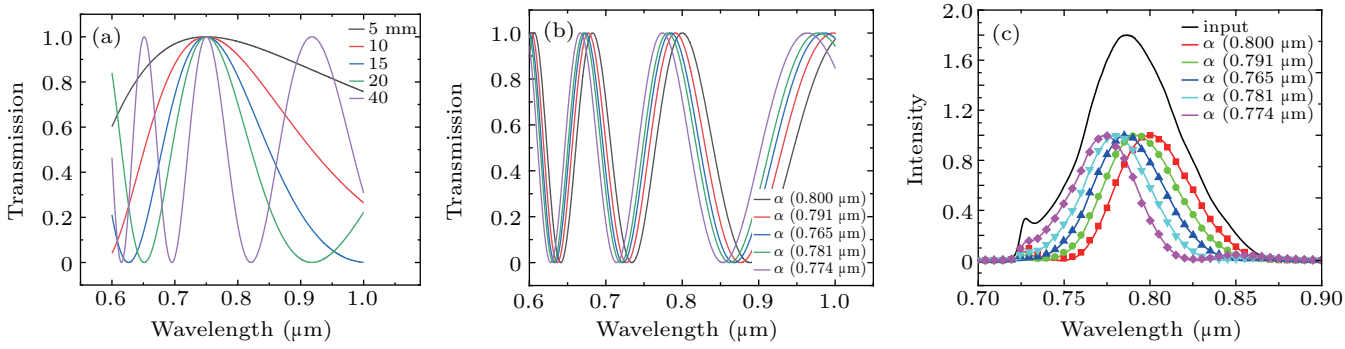


Fig. 4. (a) The transmission *versus* wavelength (in unit μm) by using a piece of quartz as ORD crystal (black: $L = 5.0$ mm; red: $L = 10.0$ mm; blue: $L = 15.0$ mm; green: $L = 20.0$ mm; purple: $L = 40.0$ mm) for a fixed $\alpha_0 = \alpha$ (0.75 μm); and (b) by using a 40-mm-thick quartz for different α_0: α (0.800 μm), α (0.791 μm), α (0.765 μm), α (0.781 μm) or α (0.774 μm); (c) theoretical and experimental results of the spectrum *versus* wavelength (μm).

However, this monotonous trend can be changed by using the combination of multiple ORD crystals. For example, if the combination consists of an $AgGaS_2$ plate and a quartz plate with a thickness ratio of 1:5.1, the ORD will exhibit parabolic-like profile (the green line in Fig. 5). The blue or red line corresponds to a thickness ratio of 1:4.0 or 1:6.0. Obviously, the ORD profile can be altered by changing the thickness ratio.

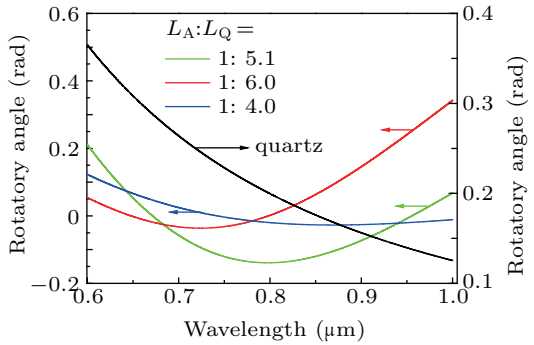


Fig. 5. The ORD $\alpha(\lambda)$ of a piece of quartz crystal (black line), a combination consisting of an $AgGaS_2$ and a quartz plate with different thickness ratios of the $AgGaS_2$ to quartz: 1:5.1 (green line), 1:6.0 (red line) or 1:4.0 (blue line).

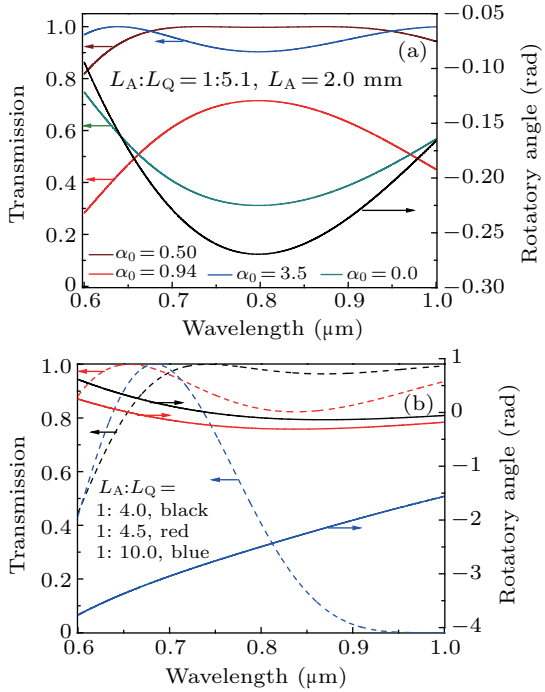


Fig. 6. The transmission *versus* wavelength (in unit μm) by using a combination of an $AgGaS_2$ plate and a quartz plate for (a) different α_0: 0.50 (purple), 0.94 (red), 3.5 (blue) or 0.0 (dark cyan) with fixed L_A: L_Q (1:5.1) and L_A (2.0 mm), and (b) for different L_A: L_Q: 1:4.0 (black), 1:4.5 (red) or 1:10.0 (blue) when $\alpha_0 = 0.0$.

In Fig. 6(a), for a given thickness ratio of the $AgGaS_2$ to the quartz plates ($L_A : L_Q = 1 : 5.1$), the parabolic ORD profile (black line) can be used to achieve not only a flat (purple line, $\alpha_0 = 0.5$) or saddle shaped (blue line, $\alpha_0 = 3.5$), but also upward (dark cyan line, $\alpha_0 = 0.0$) or downward (red line, $\alpha_0 = 0.94$) parabolic transmission from 0.6 μm to 1.0 μm by tuning α_0. For a given α_0, *e.g.* $\alpha_0 = 0.0$ as shown in Fig. 6(b), the black, red or blue line corresponds to the different thickness ratio of the $AgGaS_2$ to the quartz plates: L_A: $L_Q = 1 : 4.0$, 1:4.5 or 1:10.0 (blue), respectively, which means the transmission can also be altered by changing $L_A : L_Q$.

From the above discussions, one can see SPE allows us to flexibly manipulate spectral shaping by inducing some spectral polarization-dependent loss, which can be realized through choosing a proper combination of multi-ORD crystals, their thicknesses (the thickness ratio), and a broadband half-wave plate.

3.2. Polarization-encoded chirped pulse amplification

SPE can also help us to manipulate laser gain spectra by the aid of polarization-dependent gain. As we know, some laser crystals have broad polarization-dependent gain spectra, so SPE can be used to control the output spectrum from some lasers. It motivates us to use SPE to suppress efficiently spectral narrowing which is one of the most important but challenging works for a CPA system. Until now, the most popular laser crystal used to boost ultrashort pulse power is Ti:S whose fluorescence bandwidth is broader than 0.2 μm.[20] Even so, the serious spectral narrowing still occurs for a seed with few-cycle pulse duration. Fortunately, the Ti:S has polarization-dependent gain, which allows us to flexibly control amplified spectrum by SPE. As is known, the gain cross-section of Ti:S crystal for the π-polarized beam is about 2.4 times as large as that for the σ-polarized. Traditionally, the Ti: S amplifiers are designed to amplify their seed pulses with π-polarization for maximizing laser gain. In order to avoid the spectral narrowing, efforts are usually made to suppress the laser gain for the spectral components around the central wavelength of the seeded pulses, meanwhile, to increase the gain for those far away from the central wavelength. Correspondingly, by use of a BHW and a block of quartz crystal, we applied our SPE to a Ti:S regenerative amplifier[21] where the seed pulses are amplified with σ-polarization for the spectral components around the central wavelength, and with π-polarization for those far away from the central wavelength.

Figure 7(a) presents our calculations according to Eqs. (1) and (2) and Table 1 of Ref. [21] when using an 11-mm-thick quartz plate and setting the σ-polarization wavelength $\lambda_\sigma = 0.82$ μm. As shown by the blue solid-triangle marks, the amplified pulse bandwidth is initially 44.1 THz, and increases to 49.1 THz with the pass number N up to 30. In spite that it decreases slightly to 48.1 THz when N rises to 40, the spectral narrowing is efficiently avoided in the regenerative amplification with an output pulse energy of ~ 3.24 mJ. However, σ-polarization amplification for the spectral components around the central wavelength implies some sacrifices of amplification efficiency. Consequently, amplification saturation occurs at pass number $N \approx 40$ as shown by the black marks.

Furthermore, if a combination consisting of a quartz plate and an $AgGaS_2$ plate is used instead of a single quartz plate as

the optically rotatory disperser, the ORD profile can become parabolic, so we can set two wavelengths on the opposite sides relative to the wavelength with π-polarization and the spectral components around the central wavelengths to be amplified away from π-polarization. In Fig. 7(b), we make numerical simulation basing on the layout in Fig. 1(a) of Ref. [21] with the same equations and initial specifications of Fig. 7(a). The thicknesses of the used $AgGaS_2$ plate and quartz plate are 8 mm and 47 mm respectively, and the two π-polarized wavelengths are set at 0.69 μm and 0.95 μm by rotating the BHW. Figure 7(b) shows the amplifier can still boost the output pulses up to 3.28 mJ without spectral narrowing, but N reduces to 30 for amplification saturation, which means the amplification efficiency has been greatly improved compared with that of Fig. 7(a).

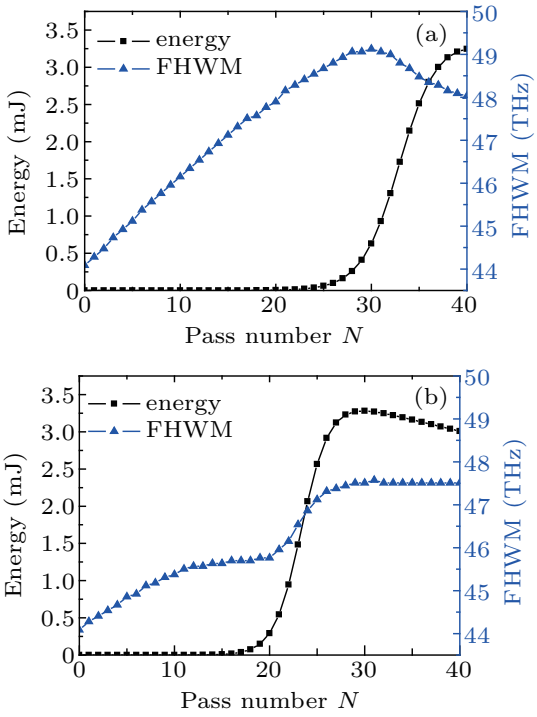


Fig. 7. The evolutions of the amplified bandwidth and pulse energy *versus* pass number N of the seed through Ti:S regenerative amplifier shown in Fig. 1 of Ref. [18] with (a) an 11 mm-thick quartz plate and $\lambda_\sigma = 0.82$ μm, and with (b) an 8 mm $AgGaS_2$ plate plus a 47 mm quartz plate and $\lambda_{\pi1} = 0.69$ μm, $\lambda_{\pi2} = 0.95$ μm.

In a Ti:S multi-pass amplifier, we have also set two π-polarized wavelengths ($\lambda_{\pi1}$ and $\lambda_{\pi2}$) by using a block of quartz plate to induce ORD,[22] where the π-polarized wavelength $\lambda_{\pi1}$ for the odd-numbered amplification is different from $\lambda_{\pi2}$ that for the even-numbered amplification, and $\lambda_{\pi1}$ and $\lambda_{\pi2}$ are on the opposite sides relative to the wavelength with maximal gain. Calculations show our design can also amplify a 0.8-μm, 10-fs seed pulse from sub-nJ to more than 3 mJ without spectral narrowing. What is more, proper ORD allows the setup to output its spectrum to be as broad as 0.149 μm.

The validity of our SPE to manipulate laser gain spectra was experimentally confirmed in a multi-pass[23] and a regenerative[24] amplification systems, where nearly 90-nm broadband amplification was achieved. According to the results described above, our SPE may open a promising way to few-cycle PW-class laser system.

3.3. Application in tunable mid-IR lasers

Obviously, SPE, which can be used to manipulate laser gain/loss, can be also applied for laser tunning. In recent years, 3 μm–5 μm mid-IR lasers begin to draw considerable attention due to a variety of important applications in biomedical, material processing, remote sensing, target detection, and other fields. However, compared with those in near-IR and visible regions, the components, *e.g.*, grating and prism in mid-IR region are much more immature and expensive which are dragging the development of mid-IR tunable laser. Fortunately, SPE allows us to realize the wavelength tunability for a mid-IR laser by just a piece of ORD with good transmission in mid-IR region.

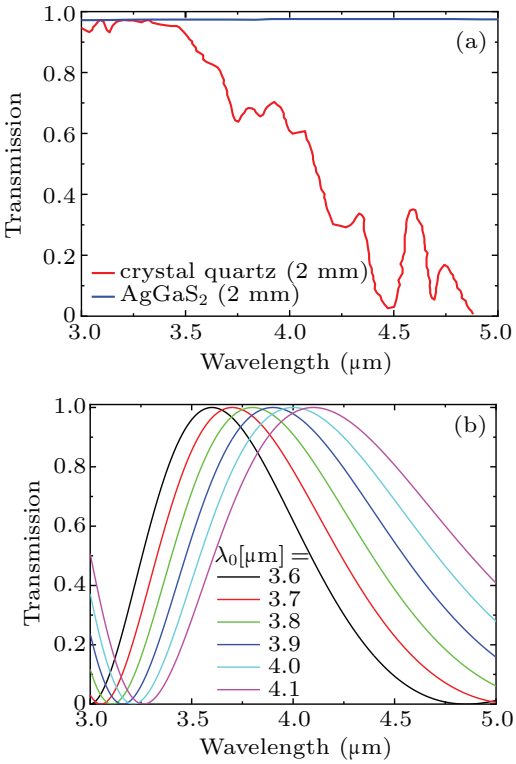


Fig. 8. (a) The transmission of quartz and $AgGaS_2$ in 0 μm–5 μm;[25,26] (b) The transmission *versus* 1/wavelength (1/μm) by using a 15-cm $AgGaS_2$ as ORD crystal.

According to the data from Terahertzlabs, Inc.,[25,26] figure 8(a) presents the transmittance of quartz and $AgGaS_2$ with a thickness of 2 mm. We can see the transmittance curve of $AgGaS_2$ almost kept a constant of $\sim 97\%$ ranging from 3 μm to 5 μm without consideration of Fresnel loss. By contrast, the transmittance of the quartz begins to decrease, and drops to 50% at 4.0 μm.

Similar to the calculations in Fig. 4, figure 8(b) shows the polarization-dependent transmission of a setup according

to Fig. 3 with a 15-cm $AgGaS_2$ as the ORDC for different maximal transmission wavelengths: 3.6, 3.7, 3.8, 3.9, 4.0, and 4.1 μm, which can be tuned by adjusting the angle of half-wave plate as mentioned above. From Fig. 8, $AgGaS_2$ is expected to be a promising candidate for wavelength tunning in mid-IR laser.

4. Conclusions

In this paper, a kind of spectral polarization-encoding, or SPE, is proposed for ultrashort light pulses by inducing ORD from some optically active crystals. SPE encodes all the spectral components of a linearly polarized ultrashort pulse with different polarization directions, and can decoded by compensating the corresponding ORD, which is easily realized not only by using a double-pass design, two optically rotatory dispersers with mirror-symmetrical configurations, but also by a combination of another same optically rotatory disperser plus a broadband half-wave plate. By using some ORD crystals plus a linear polarizer, SPE can work to manipulate polarization-dependent transmission for central wavelength or bandwidth-tunable filtering through inducing spectral polarization-dependent loss. SPE can also induce polarization-dependent gain by the aid of some broad polarization-dependent laser media. Applying our SPE to a Ti:S amplifier, we can boost a 0.8-μm nJ-pulse up to mJ level with a bandwidth to support few-cycle pulse duration. This SPE is entirely passive thus very simple to design and align, so it can be used to realize flexibly mid-IR tunable laser beyond 3 μm by using an ORD crystal with a good transmission, *e.g.* $AgGaS_2$, where the tunning devices are rather under developed compared with those in visible and near-infrared region.

References

[1] Sun S, Li M, Tang J, Zhu N, Ahn T and Azaña J 2016 *Opt. Express* **24** 7943
[2] Zohreh L, Valentina C, Karsten R, Michael G and Christophe P 2015 *Fiber Integrated Opt.* **34** 23
[3] Salem R, Foster M A and Gaeta A L 2013 *Adv. Opt. Photon.* **5** 274
[4] David C, Pedro A and Enrique S 2013 *Opt. Express* **21** 28550
[5] Stoll T, Maioli P, Crut A, Fatti N D and Vallée F 2014 *Eur. Phys. J. B* **87** 260
[6] Suzuki T, Hida R, Isa F, Ueda R and Kannari F 2016 *Imaging and Applied Optics* IW1E.3
[7] Zhang J, Zhang W and Yao J 2015 *J. Lightwave Technol.* **33** 4622
[8] Yang J, Zhou W, Dong D, Zhang Z, Lao Da, Ji R and Wang D 2016 *Proc. SPIE* **9903** 990307
[9] Zhang Z, Balskus K, McCracken R A and Reid D T 2015 *Opt. Lett.* **40** 2692
[10] Mishra A, Karni O and Eisenstein G 2015 *Opt. Express* **23** 29940
[11] Pálfalvi L, Ollmann Z, Tokodi L and Hebling J 2016 *Opt. Express* **24** 8156
[12] Jovanovic I, Ebbers C A and Barty C P J 2002 *Opt. Lett.* **27** 1622
[13] Chu Y, Gan Z, Liang X, Yu L, Lu X, Wang C, Wang X, Xu L, Lu H, Yin D, Leng Y, Li Rand Xu Z 2015 *Opt. Lett.* **40** 5011
[14] Frumker E and Silberberg Y 2007 *Opt. Lett.* **32** 1384
[15] García-Muñoz V, Preciado M A and Muriel M A 2007 *Opt. Express* **15** 10878
[16] Aoyama M, Yamakawa K, Akahane Y, Ma J, Inoue N, Ueda H and Kiriyama H 2003 *Opt. Lett.* **28** 1594
[17] Antonuccia L, Rousseaua J P, Julliena A, Merciera B, Laudeb V and Cheriauxa G 2009 *Opt. Commun.* **282** 1374
[18] Leng Y, Lin L, Wang W, Jiang Y, Tang B and Xu Z 2003 *Opt. Fiber Technol.* **35** 425
[19] Oksenhendler T, Kaplan D, Tournois P, Greetham G M and Estable F 2006 *Appl. Phys. B* **83** 491
[20] Moulton P F 1986 *J. Opt. Soc. Am. B* **3** 125
[21] Zheng S, Cai Y, Zeng X, Zheng G, Lu X, Li J and Xu S 2015 *Laser Phys. Lett.* **12** 085301
[22] Zheng S, Zeng X, Pan X, Li J, Cai Y, Zheng G and Xu S 2016 *Opt. Laser Eng.* **78** 86
[23] Kalashnikov M, Cao H, Osvay K and Chvykov V 2016 *Opt. Lett.* **41** 25
[24] Wang X, Lu X, Xu Y, Wang C, Li S, Yu L, Liu X, Liu K, Xu R and Leng Y 2018 *Appl. Phys. Express* **11** 062701
[25] http://terahertzlabs.com/Pros_View.aspx?classId=103&id=317
[26] http://terahertzlabs.com/Pros_View.aspx?classId=103&id=282